A potential lignocellulosic biomass based on banana waste for critical rare earths recovery from aqueous solutions

Byron Lapo[a,b*], Jordi J. Bou[a], Javier Hoyo[c], Manuel Carrillo[d], Karina Peña[d], Tzanko Tzanov[c] and Ana María Sastre[a]

[a]Universitat Politècnica de Catalunya, Department of Chemical Engineering, ETSEIB, Diagonal 647, 08028 Barcelona, Spain

[b]Universidad Técnica de Machala, School of Chemical Engineering, UACQS, BIOeng, 070151 Machala, Ecuador.

[c]Grup de Biotecnologia Molecular i Industrial, Department of Chemical Engineering, Universitat Politècnica de Catalunya, Rambla Sant Nebridi 22, 08222, Terrasa, Spain

[d]National Institute of Research INIAP, Soil Laboratory, Quevedo, Ecuador.

*__Corresponding author:__ Byron Lapo, Universitat Politècnica de Catalunya, Department of Chemical Engineering, ETSEIB, Diagonal 647, 08028 Barcelona, Spain. E-mail: byron.lapo@upc.edu

Abstract

Rare earth elements (REE) present multiple applications in technological devices but also drawbacks (scarcity and water contaminant). The current study aims to valorise the banana wastes - banana rachis (BR), banana pseudo-stem (BPS) and banana peel (BP) as sustainable adsorbent materials for the recovery of REE (Nd^{3+}, Eu^{3+}, Y^{3+}, Dy^{3+} and Tb^{3+}). The adsorbent materials were characterized using analytical techniques such as: Fourier transform infrared spectroscopy, X-ray photoelectron spectroscopy, zeta potential and scanning electron microscopy with energy dispersive X-ray probe. The adsorption performance and mechanisms were studied by pH dependence, equilibrium isotherms, kinetics, thermodynamics, ion-exchange and desorption evaluation. The results show good adsorption capacities for the three materials, highlighting BR that presents ~100 mg/g for most of the REE. The adsorption process (100 mg REE/L) reaches the 60% uptake in 8 minutes and the equilibrium within 50 minutes. On the other hand, the thermodynamic study indicates that the adsorption is spontaneous and exothermic ($\Delta H^{\circ} < 40$ KJ/mol). The adsorption mechanism is based on the presence of carboxylic groups that induce electrostatic interactions and facilitate the surface nucleation of REE microcrystals coupled to an ion exchange process as well as the presence of other oxygen containing groups that establish weak intermolecular forces. The recovery of REE from the adsorbent (~ 97 %) is achieved using EDTA as desorbing solution. This research indicates that banana waste and particularly BR is a new and promising renewable bioresource to recover REE with high adsorption capacity and moderated processing cost.

Keywords: adsorption; banana waste; biosorption; ion-exchange; electrostatic attraction

1. Introduction

Rare earth elements (REE) present huge applications as catalysers and in technological devices such light-emitting diodes, lasers, electronic video displays, magnet, glass polishing, ceramics, metallurgical additives and alloys, among others (Song et al., 2013). Considered as strategic resources, REE such as neodymium (Nd^{3+}), europium (Eu^{3+}), yttrium (Y^{3+}), dysprosium (Dy^{3+}) and terbium (Tb^{3+}) have been listed as critical elements, due to the possible scarcity and supply dependence in the near future (U.S. Department of Energy, 2012). Moreover, some environmental issues associated with REE processing have been reported as responsible for water and soil contamination, human and animal poisoning, soil degradation and radioactivity potential (Rim et al., 2013). Therefore, governmental and private institutions are making many efforts in developing technologies to recycle the REE from used devices.

Several technologies, frequently applied after solid-liquid extraction, including flotation, coagulation, flocculation, solvent extraction, ion exchange, coprecipitation and adsorption have been developed for REE recovery (Negrea et al., 2018). Adsorption is the most promising technology to separate metals and REE from the aqueous phase due to the simplicity of the process and the possibility of using natural or biological adsorbents (Anastopoulos et al., 2016), resulting in low-cost and sustainable processes. For instance, Eu^{3+} was removed from water with malt spent rootlets (Anagnostopoulos and Symeopoulos, 2013), cactus fibres (Prodromou and Pashalidis, 2016), crab shells (Cadogan et al., 2014) and bone powder (Butnariu et al., 2015). Y^{3+} was removed using Pleurotus Ostreatus (Hussien and Desouky, 2014) and durian rind waste (Kusrini et al., 2019). Tb^{3+} was adsorbed with poplar biomass (Demey et al., 2019), while the recovery of Dy^{3+} has not been explored using bioresourced materials.

Most of the described materials are poorly available and presented low adsorption capacity (~ 50 mg/g), which points the need of sustainable adsorbent materials such as lignocellulosic wastes. -grapefruit peel, pineapple crown and orange peel- which were used for non-critical REE removal - Ce^{3+}, La^{3+} and Pr^{3+}- (Anastopoulos et al., 2016). Banana plant waste represent an excellent bioresourced adsorbent material that is massively produced after each harvesting (9 months) (Robinson and Galán Saúco, 2010). Banana is cultivated in more than 130 countries and produces 144 million metric tons of fruits per year (Ahmad and Danish, 2018). Banana wastes (BW) include banana rachis (BR), banana pseudo-stem (BPS), banana peel (BP) and leaves. Every tonne of harvested banana fruit generates 3 tonnes of BPS, 300 kg of BP and 150 kg of BR, (Guerrero et al., 2016). The applications of these parts include bio-adsorbents of environmental pollutants such as heavy metals (Anwar et al., 2010), dyes (Amela et al., 2012), organics (Kong et al., 2016), pesticides (Salman and Hameed, 2010), anions (Mondal, 2017) and some actinides (Oyewo et al., 2016). Nevertheless, despite the reported applications, they have not been tested for REE adsorption, and remarkably BR has not been considered as an adsorbent material for any element or compound.

This research is focused on the recovery of the five catalogued critical REE (Nd^{3+}, Eu^{3+}, Y^{3+}, Dy^{3+} and Tb^{3+}) from aqueous solutions using three main BW: BR, BPS and BP as adsorbent materials. The process is optimized in lab scale and the main adsorption mechanisms are elucidated, demonstrating for the first time the application of lignocellulosic materials for critical REE removal. According to this research, BW and in particular BR represents a novel, renewable and efficient bioresource for REE adsorption.

2. Materials and Methods

2.1. Materials and chemicals

The adsorbents consisted of three banana (*Musa Cavendish*) waste materials: BR, BPS and BP, which were collected from a farm located in the south of Ecuador (3°14´S, 79°51´W). The materials were processed immediately after the fruit harvesting. They were washed, chopped in small pieces of about 2-4 cm^3, dried into a forced air convection oven at 45 ºC, milled and sieved at particle size from 250 to 800 µm. Finally, these particles in this fraction were air-dried (45ºC) and stored in plastic bottles for further experimentation.

Neodymium (III) nitrate hexahydrate ($Nd(NO_3)_3.6H_2O$, 99.9% Alfa Aesar), yttrium(III) oxide (Y_2O_3, 99.99%, Sigma Aldrich), europium(III) oxide (Eu_2O_3, 99.99%, Sigma Aldrich), dysprosium(III) nitrate pentahydrate ($Dy(NO_3).5H_2O$, 99.9%, Alfa Aesar) and terbium(III) chloride hexahydrate ($TbCl_3.6H_2O$, 99.99%, Alfa Aesar) were used to prepare the stock solutions. Milli-Q water was used to prepare all the solutions.

2.2. Material characterization

The quantity of cellulose and hemicellulose in the BW was measured by the application of ASTM D-1103-60 and ASTM D-1104-56 standard methodology respectively. Lignin content was determined by TAPPI 222 om-02 standard (TAPPI, 2006). Additionally, Fourier transform infrared (FTIR) spectra were recorded from 450 cm^{-1} to 4000 cm^{-1} to determine the functional groups of the BW materials in a FTIR-ATR spectrometer (Perkin Elmer, Spectrum Two). X-ray Photoelectron Spectroscopy (XPS) analysis were performed in a SPECS XPS system (XR-50 dual anode operating with Al source at 250 W) and PHOIBOS 150 MCD-9 detector using a pass energy of 20 eV with steps of 1 eV

for survey analysis and 0.1 eV for high resolution spectra. Total acid, carboxylic, lactonic and phenolic group concentrations were determined by Boehm titration according to Goertzen et al. (Goertzen et al., 2010). Zeta potential surface values were obtained in a Zetasizer Nano Z (Malvern Instruments Inc.) adding 1 g/L of particles in solutions of NaCl 0.001 M at different pH. Moreover, pH point of zero charge (pH_{pzc}) was measured according to Lapo et al. (Lapo et al., 2018).

Scanning electron microscope (SEM) surface morphology images were performed in a Phenom XL microscope equipped with an energy dispersive X-ray probe (EDX). The materials before and after REE adsorption were dried and sputtered with a carbon film prior to the SEM-EDX analysis.

2.3. Adsorption experiments

2.3.1 Adsorption pH dependence

To establish the suitable pH at which the adsorption of REE achieves the highest performance, adsorption experiments at different initial pHs were carried out by triplicate. 25 mg of the sorbent material was added to each 25 mL of solution (sorbent dosage (SD): 1g sorbent material/L) of initial concentration (C_i) of 100 mg/L of Nd^{3+}, Eu^{3}, Y^{3+}, Dy^{3+} and Tb^{3+}, respectively and initial pH (pH_i) of 2.0, 3.0, 4.0, 4.5 and 5.0. Then, the flasks were placed in an orbital shaker at agitation speed (AS) of 150 rpm for 24 h of contact time (CT) at room temperature (T: 22ºC). The metal concentration after the adsorption was measured in an inductively coupled plasma - optical emission spectroscopy (ICP-OES, Perkin Elmer Optima). The optimal pH is based on the uptake adsorption capacity (q_e) calculated according to the equation 1.

$$q_e = \frac{(C_i - C_e)V}{m} \quad (1)$$

Where q_e is the equilibrium uptake adsorption capacity (mg/g), C_i is the initial concentration (mg/L), C_e is the equilibrium concentration (mg/L), V is the volume (L) and *m* is the adsorbent material mass (g).

For statistical purposes, all the experiments were carried out by triplicated and the error bars values were calculated.

2.3.2 Equilibrium study

The equilibrium experiments were performed varying the C_i of REE concentration from 10 to 300 mg/L while maintaining constant the SD at 1 g/L, T:22 ºC, AS: 180 rpm, CT: 24 h and pH_i 4.5. The equilibrium isotherms were modelled by the application of Langmuir, Freundlich and Dubinin-Radushkevich (R-D) nonlinear models, according to the equations 2, 3 and 4 respectively:

Langmuir non-linear equation:

$$q_e = \frac{q_{max} b C_e}{1 + b C_e} \quad (2)$$

Freundlich non-linear equation:

$$q_e = K_F C_e^{1/n} \quad (3)$$

Dubinin-Radushkevich (D-R) non-linear equation:

$$q_e = (q_s)\exp(-K_{DR}\varepsilon^2) \quad (4)$$

Where q_e is the amount of metal adsorbed in (mg/g), C_e is the equilibrium concentration in (mg/L), q_{max} is the Langmuir adsorption maximum capacity expressed in (mg/g), b is the Langmuir constant in (L/mg), K_F is the Freundlich constant ($mg^{1-1/n}/g\ L^{1/n}$), *n* is sorption intensity (dimensionless), q_s is the D-R constant (mg/g), K_{DR} is a constant

155 related to the mean free energy of adsorption per mole of the adsorbate (mol^2/kJ^2) and ε
156 is the Polanyi potential (J/mol), which is equal to $RT\ ln\left[1 + (\frac{1}{C_e})\right]$, where R (J/mol K) is
157 the gas constant and T (absolute temperature, K).

158 The mathematical modelling of the equilibrium isotherms was performed using
159 MATLAB R2018b.

160 **2.3.3 Ion exchange evaluation**

161 BW are lignocellulosic materials that contain elements such as K, Ca, Mg and Si that
162 can present ion exchange properties (Jeon et al., 2007) with aqueous solutions
163 containing REE. Therefore, to evaluate the relevance of ion exchange mechanism in the
164 REE uptake, the concentrations of K^+, Ca^{2+}, Mg^{2+} and Si^{4+} ions released in aqueous
165 phase were measured before and after the BW materials and REE contact. For this
166 evaluation, 0.05 g of each BW was added to 50 mL of REE solution SD: 1 g/L. The
167 experimental conditions for ionic exchange were C_i: 100 mg/L of each REE, pH_i 4.5, T:
168 22 ºC, AS: 180 rpm, CT: 24 h, SD: 1 g/L, n: 3. Control experiments were performed
169 using the same procedure using solutions without presence of REE. To evaluate the ion
170 exchange role, the equation (5) was applied:

$$I_{IE} = \frac{(C_R - C_B)V}{MW_{IE} * m} \quad (5)$$

171 Where I_{IE} is the molar quantity of each ion (K^+, Ca^{2+}, Mg^{2+} and Si^{4+}) involved in ion
172 exchange reaction by mass of BW expressed in mmol/g, C_R is the concentration in mg/L
173 of each ion released (K^+, Ca^{2+}, Mg^{2+} and Si^{4+}) into the solutions after REE contact, C_B is
174 the concentration of each ion (K^+, Ca^{2+}, Mg^{2+} and Si^{4+}) in the blank experiment, V is the
175 solution volume (L) in which the experiment was carried out, MW_{IE} is the molar mass

176 expressed in (mg/mmol) of each ion evaluated and m is the mass of the BW in grams.
177 On the other hand, the molar quantity of REE adsorbed was calculated by the
178 application of the equation (6).

$$A_{REE} = \frac{(C_i - C_e)V}{MW_{REE} * m} \quad (6)$$

179 Where A_{REE} is the molar quantity of each REE adsorbed per mass unit of BW (mmol/g),
180 C_i and C_e are the initial and equilibrium concentrations respectively in (mg/L) of each
181 REE, V is the solution volume (L), MW_{REE} is the molar mass in (mg/mmol) of each
182 REE evaluated and m is the mass of the BW in grams.

183 **2.3.4 Kinetic study**

184 Adsorption kinetics were studied in individual solutions of Nd^{3+}, Eu^{3+}, Y^{3+}, Dy^{3+} and
185 Tb^{3+} of C_i of 100 mg/L using BR. It was added 500 mg of BR into 500 mL (SD 1 g/L)
186 of adjusted pH 4.5 solutions of REE. The data were adjusted using nonlinear equations
187 of pseudo first order (PFORE), pseudo second order (PSORE) and Elovich models
188 according to equations 7, 8, 9 respectively (Tan and Hameed, 2017).

189 Pseudo-first order rate equation (PFORE):

$$\frac{dq}{dt} = k_1(q_e - q) \quad (7)$$

190 Pseudo-second order rate equation (PSORE):

$$\frac{dq}{(q_e - q)^2} = k_2 dt \quad (8)$$

191 Elovich equation:

$$q = \frac{1}{\beta} \ln (1 + \propto \beta t) \quad (9)$$

Where q_e is the equilibrium sorption capacity (mg/g), q is the sorption capacity (mg/g), t (time, min), k_1 is the PFORE rate constant (1/min), k_2 is the PSORE rate constant (g/mg·min), α is the initial adsorption rate (mg/g·min), β (mg/g) is a desorption constant related to the extent of surface coverage and activation energy.

The mathematical modelling of the kinetics studies was performed using MATLAB R2018b.

2.3.5 Thermodynamics

Three sets of equilibrium isotherms at different temperatures (22ºC -room-, 35ºC and 45ºC were carried out at the same conditions indicated in section 2.3.2. The ΔG^o was calculated according to equation 10:

$$\Delta G^o = -RTlnK_C \tag{10}$$

ΔH^o and ΔS^o were calculated from the slope and intercept of the linear adjustment from the plot of ln K_c versus 1/T, following the Van't Hoff equation (11):

$$\ln K_C = \frac{-\Delta H^o}{R} * \frac{1}{T} + \frac{\Delta S^o}{R} \tag{11}$$

Where ΔG^o, ΔH^o and ΔS^o are the standard free energy, enthalpy and entropy changes, R is the universal gas constant (8.3144 J/mol K), T is the absolute temperature (K) and K_c is the dimensionless constant calculated from the $10^6 \cdot b$ (Langmuir) constant -equation 2- (Tran et al., 2017a).

2.3.6 Desorption evaluation

To assess the REE recovery from the biomaterial, an adsorption-desorption cycle was carried out using EDTA 0.01 M and HCl 0.1 M as eluents. The recovery percentage was calculated using the equation 12:

$$\text{Recovery } \% = \frac{C_D * V_D}{(C_i - C_e) * V_A} * 100 \quad (12)$$

where C_D is the concentration (mg/L) of the desorbed REE in the eluent, C_i and C_e are the initial and equilibrium concentration of REE (mg/L) in the sample before desorption. V_D and V_A are the volume of eluent and the volume of sample before elution, respectively.

3. Results and discussions

3.1. Composition of lignocellulosic wastes

The composition of BW biomass includes mainly cellulose, hemicelluloses, lignin and ash. Cellulose was found in BR and BPS in similar quantities, while BP's cellulose represents ~ 40% of that found in the former materials. The hemicellulose and ash content were major in BR, followed by BPS and BP. Regarding lignin content, BP presents the largest content, followed by BR and BPS. In terms of secondary cell wall, which is the complex structure composed mainly by cellulose, hemicelluloses and lignin (Rebaque et al., 2017), the content in BR was higher than in BPS and BP. These results are in line with previous reported studies for BR (Florian et al., 2019; Mohapatra et al., 2010); BPS (Mohapatra et al., 2010), and BP (Oberoi et al., 2011). On the other hand, the total acid and basic components released into the aqueous phase were identified showing a larger presence of carboxylic groups in BR than in BPS or BP. Further details are found in Table S1.

3.2 Morphological characterization

The three BW materials show different structure morphology (Fig. 1). BR presents simultaneously a rough and homogenous structure and a fibrous topography. BPS presents a heterogeneous surface with fibrous structure and slightly higher roughness than BR. BP shows a grainy structure with lower roughness than BR and BPS. The EDX elemental mapping analysis (Fig. 1. bottom panel) confirm the presence of K, Ca, Mg, Si, in the three BW material surfaces.

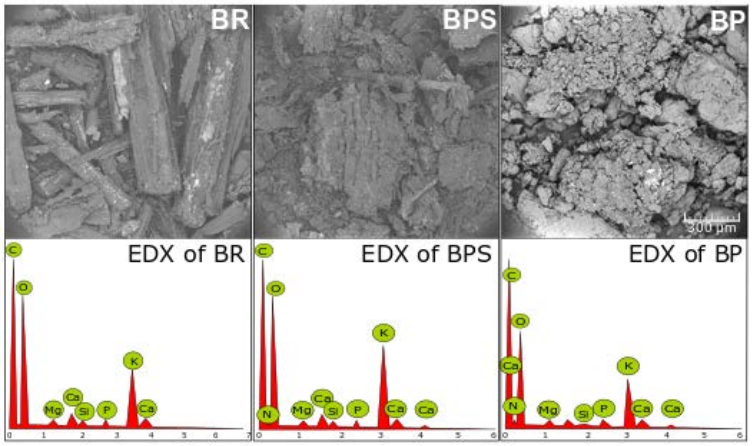

Fig. 1. Top panel: SEM representative topographical images of BR, BPS, BP. Bottom panel: elemental analysis of the corresponding top panel.

3.3 Adsorption pH dependence

The pH affects the surface of the sorbent as well as the ionic state of the chemical species in aqueous phase. The working pH range is selected to avoid the precipitation of REE over pH 6 forming $Nd(OH)_3(s)$, $Eu(OH)_3(s)$, $Y(OH)_3(s)$, $Dy(OH)_3(s)$ and $Tb(OH)_3(s)$ respectively (Fig. S1). The REE uptake capacity of the three BW materials increased as long as the pH_i was incremented (Fig. 2). In particular, BR particles show the maximum adsorption at pH_i 4.5 for all REE, while BPS and BP present a slightly better adsorption at pH_i 5.0 for most REE (Nd^{3+}, Eu^{3+}, Dy^{3+} and Tb^{3+}). On the contrary, the three materials performed the lowest adsorption at pH_i 2.0 for most of the REE. It is also important to

control that the equilibrium pH (pH_e) after the contact between the materials and the solutions containing each REE avoids the precipitation zone described above. At pH_i 5 BPS and BP materials do not reach the precipitation pH zone (Fig 2), whereas pH_i 4.5 is necessary for BR to avoid such zone. Therefore, the optimised pH for further experiments with the three BW materials is set at pH_i 4.5.

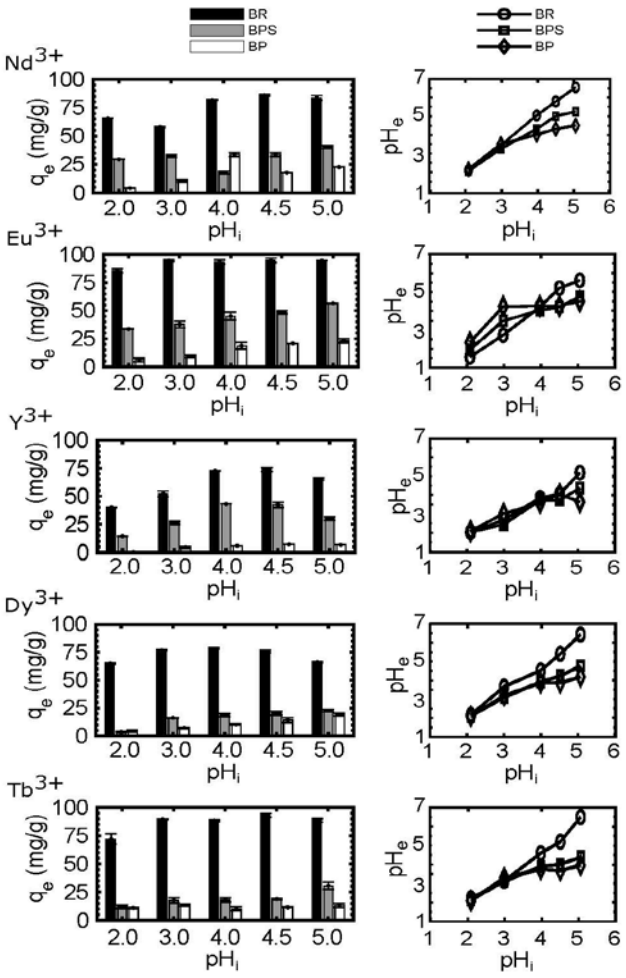

Fig. 2. Left column: Influence of pH in adsorption; right column: pH_e evolution after materials and REE solutions contact
(T: 22 °C; C_i: 100 mg/L; SD: 1 g/L; AS: 180 rpm; CT: 24 h; n=3)

The influence of electrostatic forces is crucial to explain the pH dependence phenomena in the adsorption of REE on BW. The surface ζ-potentials of the three materials at different pHs show similar trends each other (Fig. 3a), although different magnitude.

The surface ζ-potential decrease from ~0 mV to the minimum value as long as the pH was increased from pH_i 2 to pH_i 4.5 respectively. At higher pH_i (until pH 12) the surface ζ-potential remains almost constant. BR presents lower surface ζ-potential (-50 mV) at further working pH conditions (pH_i 4.5) than BPS (-35 mV) and BP (-25 mV). These differences in surface charge induce different adsorption uptake, as it is explained in section 3.6.

Furthermore, the materials pH_{pzc} values help to understand the pH influence in the adsorption of REE onto BW. The pH_{pzc} represents the pH point where the surface is in mostly neutral (Kosmulski, 2009) and over the pH_{pzc} the materials are negatively charged. The pH_{pzc} was shown at 6.5, 6.0 and 5.7 for BR, BPS and BP respectively (Fig. 3b), thus in all cases is higher than the working pH (pH_i 4.5). In addition, the pH_e observed for most of the REE and materials (Fig. 2, right column) presents a moderate increase tendency from lower to higher pH_i, which is correlated with the increase of the uptake capacity as the pH approached the pH_{pzc} (Lapo et al., 2019).

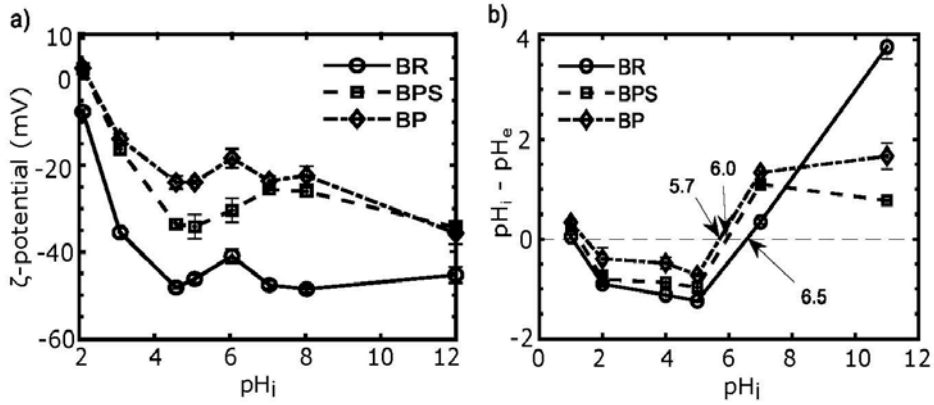

Fig. 3. a) Surface ζ-potential and b) pH_{pzc} for BW components BR, BP, BPS

3.4 Functional groups involved in the adsorption

The functional groups present in BR, BPS and BP before and after adsorption indicate the participant groups in the recovering of the REE; these aspects were elucidated by FTIR (Fig. 4) and XPS analysis (Fig. 5).

285 The three neat materials (Fig. 4a) presented intense peaks in the region of ~3300 cm^{-1}
286 corresponding to the -OH stretch, a signal at 2920 cm^{-1} attributed to methylene and
287 methyl stretching vibrations, which was stronger for BP than BPS and BR. A shoulder
288 is observed at 1723 cm^{-1} originated from C=O stretching of aldehyde or ketone groups
289 that is better resolved in BP than BPS and BR. The peak at 1591 cm^{-1} in BR, 1630 cm^{-1}
290 in BPS and 1600 cm^{-1} in BP is attributed to the asymmetric stretching of COO^-, whereas
291 the well-defined peak at 1311 cm^{-1} in BR is attributed to methylenes and alcoholic
292 bending of C-O. The strong peak at 1032 cm^{-1} present in BR, but found at 1015 cm^{-1} in
293 BPS and BP is attributed to C-O, O-C-O and C-O-C stretching and the peak at 772 cm^{-1}
294 correlates to CH_2 rocking vibration. Overall, the IR spectra of BW before the adsorption
295 is attributed to groups typically found in cellulose, hemicelluloses and lignin
296 (Guimarães et al., 2009; Hameed et al., 2008; Memon et al., 2008).
297 After REE adsorption, the three materials present an intensity reduction in all the bands
298 related with -OH, -CH, C=O, COO^- and C-O-C groups. On the other hand, it is
299 highlighted the shift of the bands at 1591 cm^{-1}, 1630 cm^{-1} and 1600 cm^{-1} in BR, BPS
300 and BP respectively to 1612 cm^{-1} and the shift from 1311 cm^{-1} to 1316 cm^{-1} for BR and
301 BPS. Altogether indicates the role of carboxylic, carboxyl, hydroxyl and ether groups
302 in the adsorption of REE; these observations were in line with previous works studying
303 the adsorption of metals onto biomaterials (Lim et al., 2008; Memon et al., 2008; Wang
304 et al., 2014). Additionally, the new bands observed at ~490 cm^{-1} and 466 cm^{-1} after the
305 REE adsorption were attributed to the stretching vibration of the complexes established
306 by the REE (Amiri and Shokrollahi, 2013).

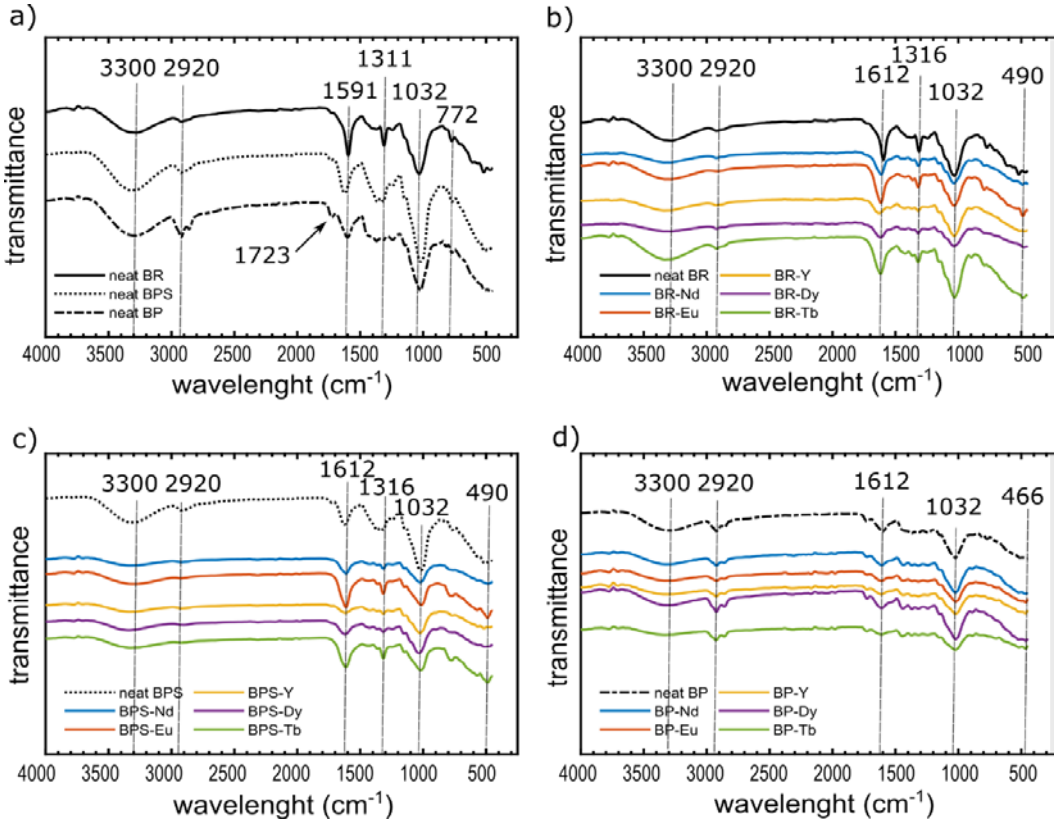

307

308 Fig. 4. FTIR spectra of a) neat BW, b) BR before and after adsorption, c) BPS before
309 and after adsorption, d) BP before and after adsorption

310

311 Core-level XPS analysis was performed (Fig. 5) to elucidate the presence of REE and the
312 groups involved in the adsorption. Nd^{3+} was chosen as the elemental representative for
313 REE adsorption for the three BW. The XPS survey of the neat materials (Fig. 5 A) shows
314 strong signals for C 1s and O 1s, and minor signals corresponding to K 2s and N 1s. After
315 adsorption, the materials show a similar profile but emerge a new signal at binding energy
316 (BE) of ~230 eV correlated with Nd $4p_{3/2}$. The elucidation at high resolution of that signal
317 is deconvoluted in three signals (Fig. 5B). The most intense peaks centred at 231.73,
318 231.64 and 231.90 eV for BR, BPS and BP respectively and is associated to Nd_2O_3
319 (Haasch et al., 2014; Sienkiewicz-Gromiuk et al., 2016), and two less intense signals
320 (~227 eV) that are attributed to $Nd(OH)_3$ (Mullica et al., 1995), and ~234 eV that is maybe
321 related to other chemical form of Nd. On the other hand, the elucidation of Nd 3d peaks

in the region of 950-1050 eV, which are normally more predominant than Nd $4p_{3/2}$ was not possible due to the overlap of O KLL Auger signal (with Al source) and C KLL signal (with Mg source) with Nd 3d signal.

The deconvolution of the core-level O 1s and C 1s (Fig. 5C and 5D) spectra indicate the interactions of Nd^{3+} with oxygen and carbon surface containing groups of the three BW. The O 1s core-level (Fig. 5C) show a marked difference after Nd^{3+} adsorption, a new signal associated to oxygen bonded to a metal (Baltrus and Keller, 2019; Oliveira et al., 2014) found at 529.6, 529.32 and 529.83 eV for BR, BPS and BP respectively - (Fig. 5C – down panel) and clearly indicate the formation of Nd_2O_3. On the other hand, the adventitious C 1s core-level was deconvoluted in four peaks at BEs of 284.8 eV, 286.4 eV, 288.0 eV and 288.63 eV that were assigned to C-C/C-H, C-O/C-O-C, C=O and O–C=O respectively (Feng et al., 2019; Lim et al., 2008). After Nd^{3+} contact, the peaks assigned to C-O/C-O-C and C=O experimented a decrease in their BE of 0.23-0.40 eV and 0.05-0.20 eV respectively, while O-C=O experimented an increase in BE (0.09-0.31 eV). Shifts in BE after metal contact are promoted by ligand electron-donor or electron-acceptor; a decrease in BE is caused by an increase in the electron density upon complex formation (Sienkiewicz-Gromiuk et al., 2016; Thomas et al., 2013). Therefore, O 1s and C 1s spectra of BW after Nd^{3+} contact confirm the participation of the oxygen functionalities, including O-C=O, C-O (ether or alcoholic) and C=O functional groups in the adsorption of REE. The major interaction in terms of BE shifts was accounted for BR followed by BPS and BP, which are in concordance with the trend in the adsorption capacity (BR>BPS>BP) – (Fig. 2).

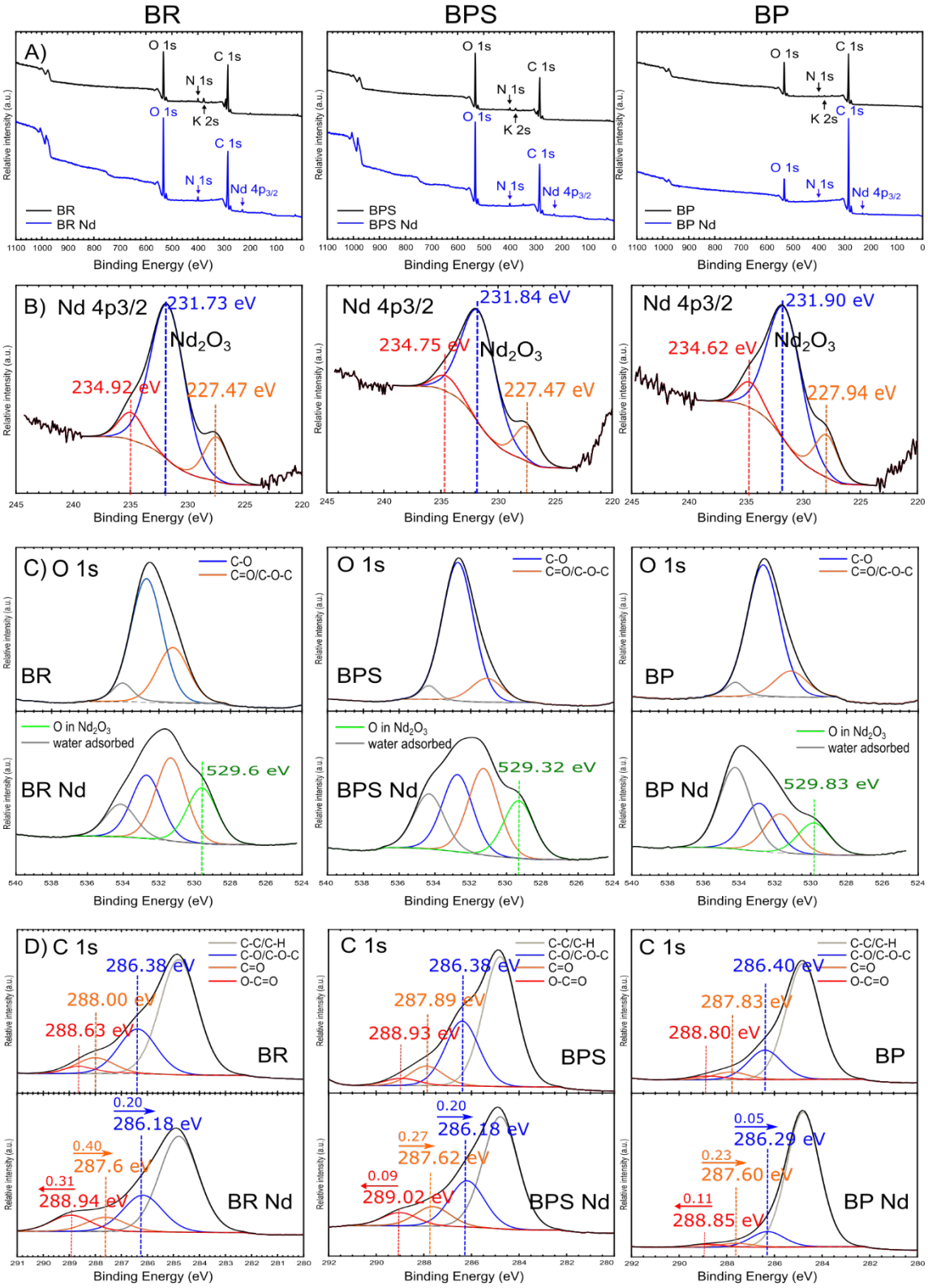

Fig. 5. XPS spectra of BR, BPS and BP showed in vertical blocs with the respective: A) XPS survey, B) high resolution Nd 4p3/2 core-level, C) high resolution O 1s core-level, D) high resolution C 1s core-level.

3.5 Adsorption isotherms

Equilibrium adsorption isotherm curves represent the phenomena between the solid-phase and aqueous environment in which a retention, release or mobility of a substance at a constant temperature and pH can occur (Limousin et al., 2007). The use of mathematical models provide physicochemical parameters describing information about the adsorption mechanisms, surface properties, sorbents affinity and the distribution of the molecules on solid phases (Foo and Hameed, 2010; Lapo et al., 2018). Among the three models evaluated (Langmuir, Freundlich and D-R), the adsorption data of REE onto BR, BP, BPS were satisfactory fitted to Langmuir or D-R models. The calculated parameters for the three models corresponding to each material are presented in Table S2. The Langmuir model (Fig. 6), the best fitting, concludes that the separation factor (R_L) was < 1 for all the studied materials in the whole range of initial concentration, indicating that the adsorption process was favourable between the three BW materials and REE (Tran et al., 2017b). Additionally, the affinity of BW materials for REE is confirmed by the high value of “b” constant of Langmuir for the three materials (Kratochvil and Volesky, 1998), which represents the steep initial sorption isotherms slope. Moreover, a plateau with the “L” shape is noted for most of the systems, with the unique exception of Dy^{3+} adsorption onto BR and BP. The achieved plateau indicates a progressive saturation of the solid and a limited adsorption capacity (Limousin et al., 2007). The D-R model (Table S2) shows low adsorption energies (<1 KJ/mol) that is associated to physisorption (Tran et al., 2016) and corroborates the electrostatic attraction discussed in section 3.6.

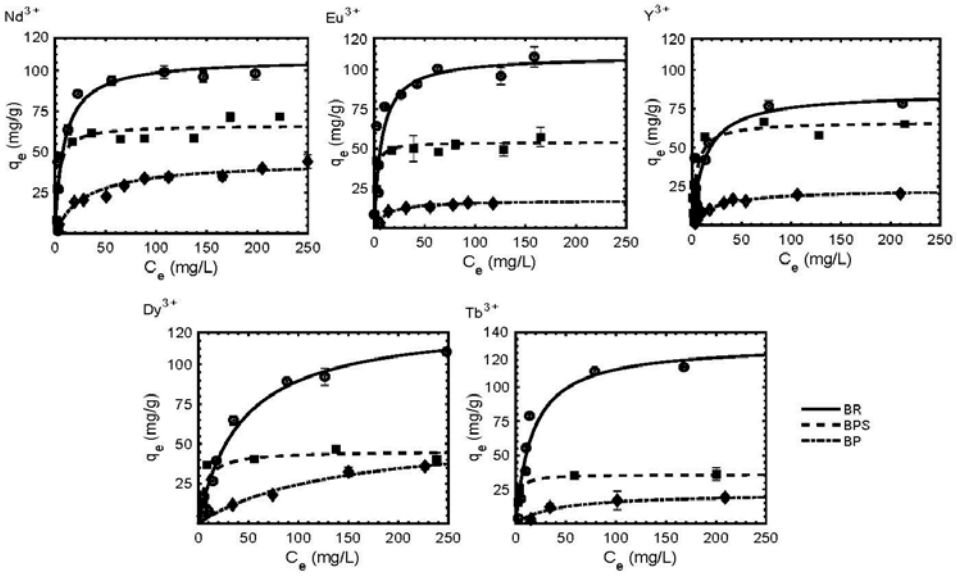

372

373 Fig. 6. Equilibrium isotherms for REE fitted to the Langmuir model
374 (T: 22 °C; C_i: 100-300 mg/L; pH_i 4.5; SD: 1 g/L; AS: 180 rpm; CT: 24 h; n = 3)
375

376 The adsorption capacity (q_{max} from Langmuir model – Table S2) of BR (~100 mg/g) is
377 higher for all the studied REE than those for BPS (~50 mg/g) and BP (< 35 mg/g). The
378 adsorption capacity of Nd^{3+}, Eu^{3+}, Dy^{3+} and Tb^{3} were higher than Y^{3+} (Fig. 6 and Table
379 S2), which was associated to the micro-precipitation observed for the former elements
380 and absence for Y^{3+} (Fig. S3, S4). The adsorption capacities of the BW materials
381 studied in the current investigation and other adsorbent biomaterials used to uptake REE
382 are presented in Table S3. BR presents higher adsorption than all the other tested
383 materials from bioresources, being its capacity only comparable to that of macroalgae
384 (Oliveira et al., 2009). BR biowaste improves the marketability of the recovering
385 process as it is low-cost, biodegradable and widely available material, which represent
386 remarkable advantages for adsorption over other extraction techniques used for metal
387 recovery/removal from aqueous phase (i.e. solid-liquid extraction, flotation,
388 coagulation, flocculation, solvent extraction, ion exchange, coprecipitation), which
389 usually require hazardous chemical reagents or complex facilities.

3.6 Adsorption mechanisms of BW derivates

At pH_i 4.5-5, the highest negative ζ-potential (Fig. 3a) correlates with the maximum adsorption uptake for all REE (Fig. 2), confirming the role of electrostatic attraction between the positively charged REE and the negatively charged surface of BW materials for the REE adsorption.

The negative surface charge of the materials is caused by the presence of carboxylic groups in their anionic form ($-COO^-$) at our working conditions. The pK_a values (2.0-5.0) of the materials are lower than the working pH, thus the deprotonation of the COOH groups and the negative charge of the surface are induced (Tran et al., 2016). In addition, the cationic metals present in the structure of the biomaterials i.e. K^+, Ca^{2+}, Mg^{2+}, Si^{4+} (Fig. 1), can be dissociated in aqueous phase, contributing to the formation of the negative material surface charge (Ding et al., 2013; Wang et al., 2014).

The adsorption uptake of REE depends directly on the surface ζ-potential value of the biomaterials (Limousin et al., 2007). In this sense, a linear correlation (Fig. S6) is observed between the surface ζ-potential (Fig. 3a) and the maximum adsorption capacity (parameter calculated by Langmuir model - Table S2) for all REE at pH_i 4.5. Therefore, the higher negative surface ζ-potential of BR particles induced higher adsorption than BPS or BP particles.

The contribution of the surface-precipitation mechanism is also relevant since it was observed for most of REE on the surfaces of BR and BPS, but not on BP particles. Fig. S2 is a representative system of those present in Fig. S3, S4, S5. The formation of microcrystals (~ 2 µm) on BR surfaces is observed after Nd^{3+} adsorption mostly accommodated between the microfibrils (Fig. S2). This phenomenon occurs with all the herein studied systems with the exception of Y^{3+}, which is in accordance with the lower

414 Y^{3+} adsorption uptake observed. The Nd EDX map (Fig. S2) confirms the Nd presence
415 along the BR surface and the EDX elemental analysis confirms the presence of Nd
416 among other elements already present in neat BR.
417 Surface-precipitation mechanism is usually driven by nucleation points provided by the
418 surface specific sites (Naja and Volesky, 2011), thus indicating that the interactions of
419 the surface functional groups of the material with the REE are mainly responsible for
420 such nucleation. The formation of micro precipitates has been previously reported for
421 rice husks with Cr(VI) (Bansal et al., 2009), crab shell particles with lanthanum
422 (Vijayaraghavan et al., 2009) and crab shell particles with lead (Lee et al., 1997).
423 The third involved adsorption mechanism was ion-exchange (Fig. 7). Ca^{2+} and Mg^{2+}
424 ions participated similarly in almost the total ion exchange produced, whereas K^{+} and
425 Si^{4+} had a minor role (Fig. 7a). In blank experiments K^{+} was released in major quantity
426 than other cations (Fig. 7b), but presented negligible participation in ion-exchange. Ca^{2+}
427 and Mg^{2+} were released in low quantities and Si^{4+} was not released in the blank
428 solution. The ion exchange capacity is associated with the arising of electrostatic forces
429 that facilitate the replacement of cations of lower oxidation number by those of higher
430 one (Ahalya et al., 2003).

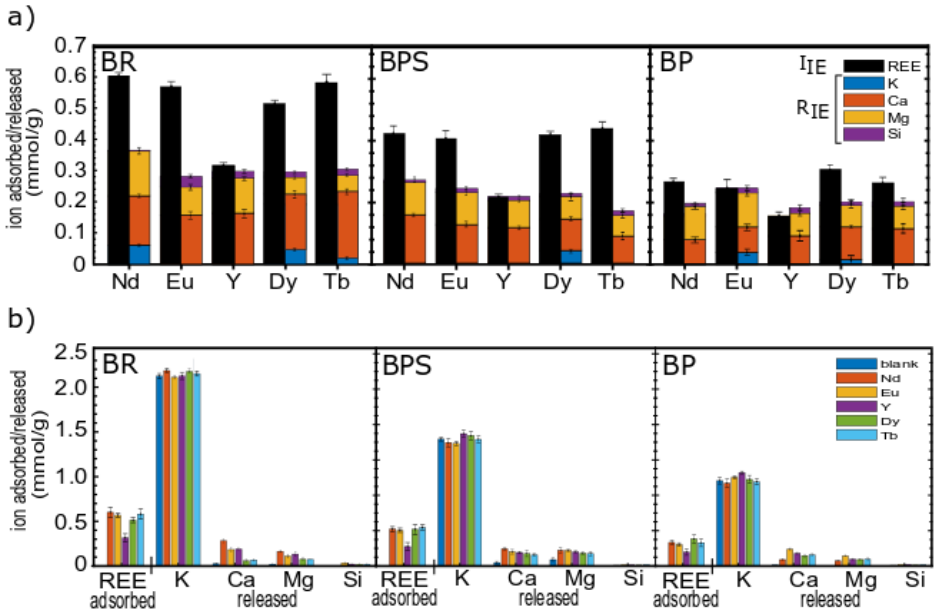

Fig. 7. Ion-exchange evaluation. a) REE adsorbed vs ion exchange, b) Individual element interactions
(T: 22 °C; C_i: 100-300 mg/L; pH_i 4.5; SD: 1 g/L; AS: 180 rpm; CT: 24 h; n = 3)

Overall, the adsorption mechanism of REE in BW is governed by the presence of deprotonated carboxylic groups that influence simultaneously the outer-sphere interactions (electrostatic) and facilitates the surface nucleation of REE microcrystals, as well as the presence of other oxygen containing groups that establish weak intermolecular forces. Additionally, the inherent presence of Ca, Mg in BW materials permits once in solution the ion exchange of these divalent cations with the REE, contributing to the global recovery of REE from aqueous solutions.

Based on the performance evaluation of the three BW, BR was selected as the best material for REE recovery. Therefore, some technological/engineering aspects were further studied on BR material in the following sections.

3.7 Kinetics

An adsorption kinetic study is crucial to establish the reactor design parameters and REE recovery process scaling up, adsorption rates and limiting mechanisms; as well as

the activation energy of the process (Lapo et al., 2019). Two pseudo-steps process are identified (Fig. 8): i) an initial film diffusion (5-8 minutes) that reached ~60% of REE adsorption and represents the transport of the adsorbate from the bulk phase to the external surface of adsorbent, and ii) an intraparticle diffusion (30-50 min) that reaches the equilibrium. The PFORE, PSORE and Elovich models (eq. 7, 8 and 9) were applied and the fitting parameters are presented in Table S4. The PSORE model presents the best fit for the data, indicating a second-order uptake rate vs. the available surface sites and pointing a diffusion-limited processes (Hubbe et al., 2019).

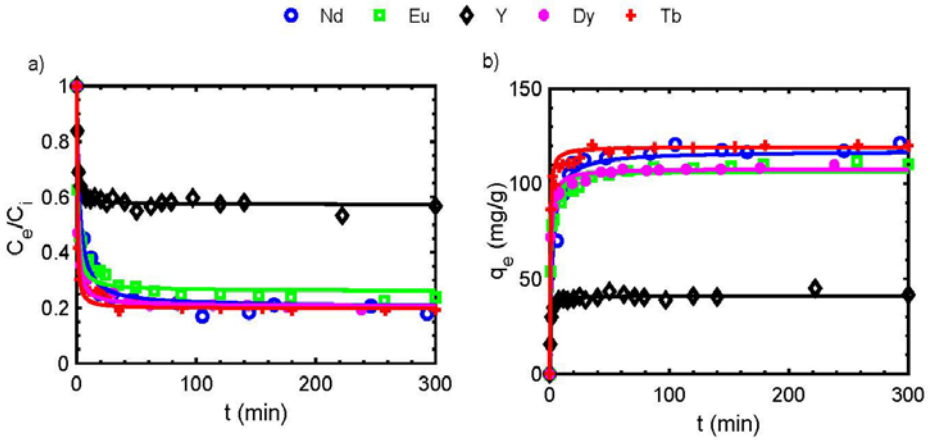

Fig. 8. Kinetics isotherms of BR. a) Concentration vs. time, b) q_e vs. time (T:22 °C; C_i: 100 mg/L; SD: 1 g/L; pH_i 4.5; AS: 180 rpm; n=3)

3.8 Thermodynamics

Thermodynamics experiments are crucial to determine if adsorption or chemisorption governs the adsorption mechanisms. Nd^{3+} was chosen as the elemental representative of the adsorption behaviour Nd^{3+}, Eu^{3+}, Dy^{3+}, Tb^{3+}. Y^{3+} was also studied due to it presented different adsorption behaviour to the abovementioned elements. Temperature increase results in lower adsorption uptake (Fig. S7), as observed for other lignocellulosic adsorbing materials, which is explained by the reduction of the number of available adsorption sites (Tran et al., 2016).

The calculated thermodynamic parameters (Table S5) indicate that the adsorption of Nd^{3+} and Y^{3+} onto BR occurred favourably and spontaneously ($\Delta G^{\circ}<0$), exothermic ($\Delta H^{\circ}<0$) and entropic ($\Delta S^{\circ}<0$). The negative ΔH° value (<40 KJ/mol) and adsorption energy (E < 0.23 KJ/mol – Table S2) indicate physisorption (Inglezakis and Poulopoulos, 2006).

3.9 Desorption

The desorption stage of REE is essential to close the recovery cycle. EDTA 0.01 M obtained (Fig. 9) the best desorption yield (up to 97%) in contrast to HCl 0.1 M (up to 38%). The excellent recovery yield observed for EDTA is mainly attributed to its chelating characteristics towards REE (Zhao et al., 2016). This almost complete elution of REE from BR confirms this material as perfect bioresourced compound for REE recovering from aqueous phase.

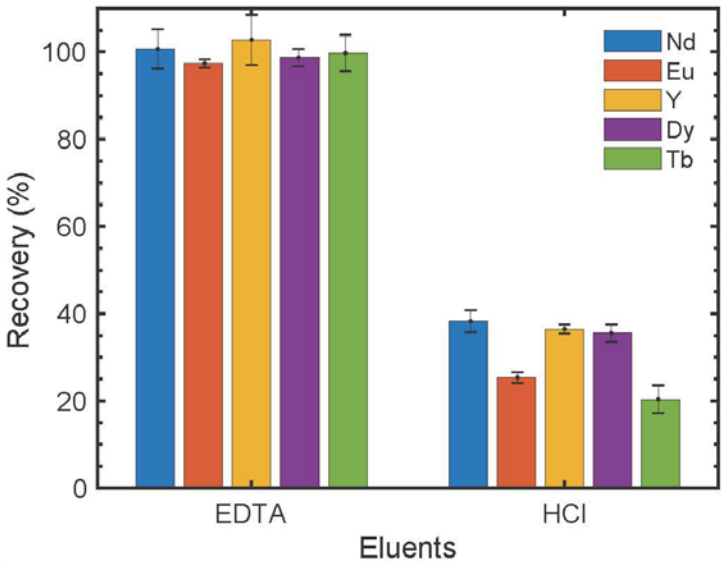

Fig. 9. REE desorption of BR using EDTA and HCl
(T: 22 °C; C_i: 100 mg/L; SD: 1 g/L; AS: 180 rpm; CT: 24 h; n=3)

4. Conclusions

BW are promising candidates for the recovery of REE from aqueous solutions using the adsorption technology. Among the BW studied herein, BR presents the highest adsorption capacity for all the studied REE, highlighting that BR presents adsorption uptake larger than 100 mg of REE/g adsorbent for most of the REE. Thus, BR is placed among the biosorbents with higher adsorption capacity. The adsorption mechanism is based on the presence of carboxylic groups that induce a combination of electrostatic interactions and nucleation points for REE microcrystals growth coupled to an ion exchange process of the inherently present cations in BR, BPS, BP, as well as other weak interactions arisen between the REE and oxygen containing groups of the BW materials. Therefore, BR has been confirmed as a low-cost and renewal bioresource for adsorption of REE through a sustainable process.

5. Acknowledgements

This work was supported by the Spanish Ministry of Economy and Competitiveness, MINECO (Project CTM2017-83581-R). The authors would like to thank to Estefania Molina from Universidad Técnica de Machala for their technical help.

Notes:

The authors declare no competing financial interest.

6. References

1. Ahalya, N., Ramachandra, T.V., Kanamadi, R.D., 2003. Biosorption of heavy metals. Res. J. Chem. Environ. 7, 484–532.
2. Ahmad, T., Danish, M., 2018. Prospects of banana waste utilization in wastewater treatment: A review. J. Environ. Manage. 206, 330–348. https://doi.org/10.1016/j.jenvman.2017.10.061
3. Amela, K., Hassen, M.A., Kerroum, D., 2012. Isotherm and kinetics study of biosorption of cationic dye onto banana peel. Energy Procedia 19, 286–295. https://doi.org/10.1016/J.EGYPRO.2012.05.208
4. Amiri, S., Shokrollahi, H., 2013. Magnetic and structural properties of RE doped Co-ferrite (RE=Nd, Eu, and Gd) nano-particles synthesized by co-precipitation. J. Magn. Magn. Mater. 345, 18–23. https://doi.org/10.1016/j.jmmm.2013.05.030
5. Anagnostopoulos, V.A., Symeopoulos, B.D., 2013. Sorption of europium by malt spent rootlets, a low cost biosorbent: effect of pH, kinetics and equilibrium studies. J. Radioanal. Nucl. Chem. 295, 7–13. https://doi.org/10.1007/s10967-012-1956-y
6. Anastopoulos, I., Bhatnagar, A., Lima, E., 2016. Adsorption of rare earth metals: A review of recent literature. J. Mol. Liq. 221, 954–962. https://doi.org/http://dx.doi.org/10.1016/j.molliq.2016.06.076
7. Anwar, J., Shafique, U., Salman, M., Dar, A., Anwar, S., 2010. Bioresource technology removal of Pb(II) and Cd(II) from water by adsorption on peels of banana. Bioresour. Technol. 101, 1752–1755. https://doi.org/10.1016/j.biortech.2009.10.021
8. Baltrus, J.P., Keller, M.J., 2019. Rare earth oxides Eu2O3 and Nd2O3 analyzed by XPS. Surf. Sci. Spectra. https://doi.org/10.1116/1.5085768

9. Bansal, M., Garg, U., Singh, D., Garg, V.K., 2009. Removal of Cr(VI) from aqueous solutions using pre-consumer processing agricultural waste: A case study of rice husk. J. Hazard. Mater. 162, 312–320. https://doi.org/10.1016/j.jhazmat.2008.05.037
10. Butnariu, M., Negrea, P., Lupa, L., Ciopec, M., Negrea, A., Pentea, M., Sarac, I., Samfira, I., 2015. Remediation of rare earth element pollutants by sorption process using organic natural sorbents. Int. J. Environ. Res. Public Health 12, 11278–11287. https://doi.org/10.3390/ijerph120911278
11. Cadogan, E.I., Lee, C.-H., Popuri, S.R., Lin, H.-Y., 2014. Efficiencies of chitosan nanoparticles and crab shell particles in europium uptake from aqueous solutions through biosorption: Synthesis and characterization. Int. Biodeterior. Biodegradation 95, 232–240. https://doi.org/10.1016/J.IBIOD.2014.06.003
12. Ding, D., Zhao, Y., Yang, S., Shi, W., Zhang, Z., Lei, Z., Yang, Y., 2013. Adsorption of cesium from aqueous solution using agricultural residue e Walnut shell : Equilibrium , kinetic and thermodynamic modeling studies. Water Res. 47, 2563–2571. https://doi.org/10.1016/j.watres.2013.02.014
13. Feng, Y., Sun, H., Han, L., Xue, L., Chen, Y., Yang, L., Xing, B., 2019. Fabrication of hydrochar based on food waste (FWHTC) and its application in aqueous solution rare earth ions adsorptive removal: Process, mechanisms and disposal methodology. J. Clean. Prod. 212, 1423–1433. https://doi.org/10.1016/j.jclepro.2018.12.094
14. Florian, T.D.M., Villani, N., Aguedo, M., Jacquet, N., Thomas, H.G., Gerin, P., Magali, D., Richel, A., 2019. Chemical composition analysis and structural features of banana rachis lignin extracted by two organosolv methods. Ind. Crops Prod. 132,

552 269–274. https://doi.org/10.1016/j.indcrop.2019.02.022
553 15. Foo, K.Y., Hameed, B.H., 2010. Insights into the modeling of adsorption isotherm
554 systems. Chem. Eng. J. 156. https://doi.org/10.1016/j.cej.2009.09.013
555 16. Goertzen, S.L., Thériault, K., Oickle, A.M., Tarasuk, A.C., Andreas, H.A., 2010.
556 Standardization of the Boehm titration. Part I. CO2 expulsion and endpoint
557 determination. Carbon N. Y. 48, 1252–1261.
558 https://doi.org/10.1016/j.carbon.2009.11.050
559 17. Guerrero, A.B., Aguado, P.L., Sánchez, J., Curt, M.D., 2016. GIS-based assessment
560 of banana residual biomass potential for ethanol production and power generation:
561 A case study. Waste and Biomass Valorization 7, 405–415.
562 https://doi.org/10.1007/s12649-015-9455-3
563 18. Guimarães, J.L., Frollini, E., da Silva, C.G., Wypych, F., Satyanarayana, K.G.,
564 2009. Characterization of banana, sugarcane bagasse and sponge gourd fibers of
565 Brazil. Ind. Crops Prod. 30, 407–415. https://doi.org/10.1016/j.indcrop.2009.07.013
566 19. Haasch, R.T., Breckenfeld, E., Martin, L.W., Breckenfeld, E., Martin, L.W., 2014.
567 Single Crystal Perovskites Analyzed Using X-ray Photoelectron Spectroscopy: 5.
568 NdGaO3(110). Surf. Sci. Spectra 3. https://doi.org/10.1116/11.20140905
569 20. Hameed, B.H., Mahmoud, D.K., Ahmad, A.L., 2008. Sorption equilibrium and
570 kinetics of basic dye from aqueous solution using banana stalk waste. J. Hazard.
571 Mater. 158, 499–506. https://doi.org/10.1016/j.jhazmat.2008.01.098
572 21. Hubbe, M.A., Azizian, S., Douven, S., 2019. Implications of Apparent Pseudo-
573 Second-Order Adsorption Kinetics onto Cellulosic Materials : A Review.
574 Bioresources 14, 7582–7626.
575 22. Hussien, S.S., Desouky, O.A., 2014. Biosorption studies on Yttrium using low cost

576 pretreated biomass of Pleurotus Ostreatus, in: 4th International Conference on
577 Radiation Sciences and Applications. pp. 13–17.
578 23. Inglezakis, V.J., Poulopoulos, S.G., 2006. Adsorption, ion exchange and catalysis :
579 design of operations and environmental applications. Elsevier.
580 24. Jeon, C., Wook, I., Hwang, K., 2007. Adsorption of heavy metals using
581 magnetically modified alginic acid 86, 140–146.
582 https://doi.org/10.1016/j.hydromet.2006.11.010
583 25. Kong, H., Cheu, S.-C., Othman, N.S., Song, S.-T., Saman, N., Johari, K., Mat, H.,
584 2016. Surfactant modification of banana trunk as low-cost adsorbents and their high
585 benzene adsorptive removal performance from aqueous solution. RSC Adv. 6,
586 24738–24751. https://doi.org/10.1039/C6RA00911E
587 26. Kosmulski, M., 2009. Surface charging and points of zero charge. CRC Press.
588 27. Kratochvil, D., Volesky, B., 1998. Advances in the biosorption of heavy metals.
589 Trends Biotechnol. 16, 291–300. https://doi.org/10.1016/S0167-7799(98)01218-9
590 28. Kusrini, E., Usman, A., Sani, F.A., Wilson, L.D., Abdullah, M.A.A., 2019.
591 Simultaneous adsorption of lanthanum and yttrium from aqueous solution by durian
592 rind biosorbent. Environ. Monit. Assess. 191. https://doi.org/10.1007/s10661-019-
593 7634-6
594 29. Lapo, B., Demey, H., Carchi, T., Sastre, A.M., 2019. Antimony removal from
595 water by a chitosan-iron (III) biocomposite. Polymers (Basel). 1–14.
596 https://doi.org/10.3390/polym11020351
597 30. Lapo, B., Demey, H., Zapata, J., Romero, C., Sastre, A.M., 2018. Sorption of
598 Hg(II) and Pb(II) ions on chitosan- iron (III) from aqueous solutions: single and
599 binary systems. Polymers (Basel). 10. https://doi.org/doi:10.3390/polym10040367

31. Lee, M.-Y., Park, J.M., Yang, J.-W., 1997. Micro precipitation of lead on the surface of crab shell particles. Process Biochem. 32, 671–677.
32. Lim, S., Zheng, Y.-M., Zou, S.-W., Chen, P., 2008. Characterization of copper adsorption onto an alginate encapsulated magnetic sorbent by a combined FT-IR, XPS and mathematical modeling study. Environ. Sci. Technol. 42, 2551–2556. https://doi.org/10.1021/es7021889
33. Limousin, G., Gaudet, J.-P., Charlet, L., Szenknect, S., Barthès, V., Krimissa, M., 2007. Sorption isotherms: A review on physical bases, modeling and measurement. Appl. Geochemistry 22, 249–275. https://doi.org/10.1016/J.APGEOCHEM.2006.09.010
34. Memon, J.R., Memon, S.Q., Bhanger, M.I., Memon, G.Z., El-Turki, A., Allen, G.C., 2008. Characterization of banana peel by scanning electron microscopy and FT-IR spectroscopy and its use for cadmium removal. Colloids Surfaces B Biointerfaces 66, 260–265. https://doi.org/10.1016/J.COLSURFB.2008.07.001
35. Mohapatra, D., Mishra, S., Sutar, N., 2010. Banana and its by-product utilisation: an overview. J. Sci. Ind. Res. 69, 323–329.
36. Mondal, N.K., 2017. Natural banana (Musa acuminate) peel: an unconventional adsorbent for removal of fluoride from aqueous solution through batch study. Water Conserv. Sci. Eng. 1, 223–232. https://doi.org/10.1007/s41101-016-0015-x
37. Mullica, D.F., Lok, C.K.C., Perkins, H.O., Benesh, G.A., Young, V., 1995. The X-ray photoemission spectra of Nd(OH)3, Sm(OH)3 , Eu(OH)3 and Gd(OH)3. J. Electron Spectros. Relat. Phenomena 71, 1–20.
38. Naja, G., Volesky, B., 2011. The mechanism of metal cation and anion biosorption, in: Kotbra, P., Mackova, M., Macek, T. (Eds.), Microbial Biorsorption of Metals.

624 Springer, pp. 19–58. https://doi.org/10.1007/978-94-007-0443-5
625 39. Negrea, A., Gabor, A., Davidescu, C.M., Ciopec, M., Negrea, P., Duteanu, N.,
626 Barbulescu, A., 2018. Rare earth elements removal from water using natural
627 polymers. Sci. Rep. 8, 1–11. https://doi.org/10.1038/s41598-017-18623-0
628 40. Oberoi, H.S., Vadlani, P. V., Saida, L., Bansal, S., Hughes, J.D., 2011. Ethanol
629 production from banana peels using statistically optimized simultaneous
630 saccharification and fermentation process. Waste Manag. 31, 1576–1584.
631 https://doi.org/10.1016/j.wasman.2011.02.007
632 41. Oliveira, R.C., García, O., Garcia Jr., O., 2009. Study of biosorption of rare earth
633 metals (La, Nd, Eu, Gd) by Sargassum sp. biomass in batch systems:
634 physicochemical evaluation of kinetics and adsorption models. Adv. Mater. Res.
635 71–73, 71–73. https://doi.org/10.4028/www.scientific.net/AMR.71-73.605
636 42. Oliveira, R.C., Hammer, P., Guibal, E., Taulemesse, J.M., Garcia, O., 2014.
637 Characterization of metal-biomass interactions in the lanthanum(III) biosorption on
638 Sargassum sp. using SEM/EDX, FTIR, and XPS: Preliminary studies. Chem. Eng.
639 J. 239, 381–391. https://doi.org/10.1016/j.cej.2013.11.042
640 43. Oyewo, O.A., Onyango, M.S., Wolkersdorfer, C., 2016. Application of banana
641 peels nanosorbent for the removal of radioactive minerals from real mine water. J.
642 Environ. Radioact. 164, 369–376. https://doi.org/10.1016/j.jenvrad.2016.08.014
643 44. Prodromou, M., Pashalidis, I., 2016. Europium adsorption by non-treated and
644 chemically modified opuntia ficus indica cactus fibres in aqueous solutions.
645 Desalin. Water Treat. 57, 5079–5088.
646 https://doi.org/10.1080/19443994.2014.1002431
647 45. Rebaque, D., Martínez-Rubio, R., Fornalé, S., García-Angulo, P., Alonso-Simón,

A., Álvarez, J.M., Caparros-Ruiz, D., Acebes, J.L., Encina, A., 2017. Characterization of structural cell wall polysaccharides in cattail (Typha latifolia): Evaluation as potential biofuel feedstock. Carbohydr. Polym. 175, 679–688. https://doi.org/10.1016/j.carbpol.2017.08.021

46. Rim, K.T., Koo, K.H., Park, J.S., 2013. Toxicological Evaluations of Rare Earths and Their Health Impacts to Workers: A Literature Review. Saf. Health Work 4, 12–26. https://doi.org/10.5491/SHAW.2013.4.1.12

47. Robinson, J.C., Galán Saúco, V., 2010. Bananas and plantains: Second edition, 2nd ed, Bananas and Plantains.

48. Salman, J.M., Hameed, B.H., 2010. Removal of insecticide carbofuran from aqueous solutions by banana stalks activated carbon. J. Hazard. Mater. 176, 814–819. https://doi.org/10.1016/J.JHAZMAT.2009.11.107

49. Sienkiewicz-Gromiuk, J., Rusinek, I., Kurach, L., Rzaczynska, Z., 2016. Thermal and spectroscopic (IR , XPS) properties of lanthanide(III) benzene-1,3,5-triacetate complexes. J. Therm. Anal. Calorim. 327–342. https://doi.org/10.1007/s10973-016-5521-8

50. Song, X., Chang, M.H., Pecht, M., 2013. Rare-earth elements in lighting and optical applications and their recycling. JOM 65, 1276–1282. https://doi.org/10.1007/s11837-013-0737-6

51. Tan, K.L., Hameed, B.H., 2017. Insight into the adsorption kinetics models for the removal of contaminants from aqueous solutions. J. Taiwan Inst. Chem. Eng. 74, 25–48. https://doi.org/10.1016/j.jtice.2017.01.024

52. TAPPI, 2006. Acid-insuble lignin in Wood and Pulp, T222 om-02. https://doi.org/10.1023/a:1019003230537

672 53. Thomas, S., Durand, D., Chassenieux, C., Jyotishkumar, P., 2013. Handbook of
673 Biopolymer-Based Materials: From Blends and Composites to Gels and Complex
674 Networks, Handbook of Biopolymer-Based Materials: From Blends and
675 Composites to Gels and Complex Networks.
676 https://doi.org/10.1002/9783527652457
677 54. Tran, H.N., You, S., Chao, H., 2017a. Insight into adsorption mechanism of
678 cationic dye onto agricultural residues-derived hydrochars : Negligible role of π - π
679 interaction 34, 1708–1720. https://doi.org/10.1007/s11814-017-0056-7
680 55. Tran, H.N., You, S.J., Chao, H.P., 2016. Thermodynamic parameters of cadmium
681 adsorption onto orange peel calculated from various methods: A comparison study.
682 J. Environ. Chem. Eng. 4, 2671–2682. https://doi.org/10.1016/j.jece.2016.05.009
683 56. Tran, H.N., You, S.J., Hosseini-Bandegharaei, A., Chao, H.P., 2017b. Mistakes and
684 inconsistencies regarding adsorption of contaminants from aqueous solutions: A
685 critical review. Water Res. 120, 88–116.
686 https://doi.org/10.1016/j.watres.2017.04.014
687 57. U.S. Department of Energy, 2012. Critical Minerals Strategy.
688 58. Vijayaraghavan, K., Mahadevan, A., Joshi, U.M., Balasubramanian, R., 2009. An
689 examination of the uptake of lanthanum from aqueous solution by crab shell
690 particles. Chem. Eng. J. 152, 116–121. https://doi.org/10.1016/J.CEJ.2009.03.040
691 59. Wang, F., Zhao, J., Wei, X., Huo, F., Li, W., Hu, Q., Liu, H., 2014. Adsorption of
692 rare earths (III) by calcium alginate-poly glutamic acid hybrid gels. J. Chem.
693 Technol. Biotechnol. 89, 969–977. https://doi.org/10.1002/jctb.4186
694 60. Zhao, F., Repo, E., Meng, Y., Wang, X., Yin, D., Sillanpää, M., 2016. An EDTA-β-
695 cyclodextrin material for the adsorption of rare earth elements and its application in

preconcentration of rare earth elements in seawater. J. Colloid Interface Sci. 465, 215–224. https://doi.org/10.1016/j.jcis.2015.11.069

7. Figure captions

Fig. 1. Top panel: SEM representative topographical images of BR, BPS, BP. Bottom panel: elemental analysis of the corresponding top panel.

Fig. 2. Left column: Influence of pH in adsorption; right column: pHe evolution after materials and REE solutions contact
(T: 22 °C; Ci: 100 mg/L; SD: 1 g/L; AS: 180 rpm; CT: 24 h; n=3)

Fig. 3. a) Surface ζ-potential and b) pHpzc for BW components BR, BP, BPS

Fig. 4. FTIR spectra of a) neat BW, b) BR before and after adsorption, c) BPS before and after adsorption, d) BP before and after adsorption

Fig. 5. XPS spectra of BR, BPS and BP showed in vertical blocs with the respective: A) XPS survey, B) high resolution Nd 4p3/2 core-level, C) high resolution O 1s core-level, D) high resolution C 1s core-level.

Fig. 6. Equilibrium isotherms for REE fitted to the Langmuir model
(T: 22 °C; Ci: 100-300 mg/L; pHi 4.5; SD: 1 g/L; AS: 180 rpm; CT: 24 h; n = 3)

Fig. 7. Ion-exchange evaluation. a) REE adsorbed vs ion exchange, b) Individual element interactions

(T: 22 °C; Ci: 100-300 mg/L; pHi 4.5; SD: 1 g/L; AS: 180 rpm; CT: 24 h; n = 3)

Fig. 8. Kinetics isotherms of BR. a) Concentration vs. time, b) q_e vs. time
(T:22 °C; Ci: 100 mg/L; SD: 1 g/L; pHi 4.5; AS: 180 rpm; n=3)

Fig. 9. REE desorption of BR using EDTA and HCl
(T: 22 °C; Ci: 100 mg/L; SD: 1 g/L; AS: 180 rpm; CT: 24 h; n=3)